UC Davis
UC Davis Previously Published Works

Title

Collapse of superconductivity in cuprates via ultrafast quenching of phase coherence.

Permalink

Journal

ISSN

Authors

Boschini, F
da Silva Neto, EH
Razzoli, E
et al.

Publication Date

DOI

Collapse of superconductivity in cuprates via ultrafast quenching of phase coherence

F. Boschini[1,2]*, E. H. da Silva Neto[1,2,3,4], E. Razzoli[1,2], M. Zonno[1,2], S. Peli[5,6], R. P. Day[1,2], M. Michiardi[1,2,7], M. Schneider[1,2], B. Zwartsenberg[1,2], P. Nigge[1,2], R. D. Zhong[8], J. Schneeloch[8,9], G. D. Gu[8], S. Zhdanovich[1,2], A. K. Mills[1,2], G. Levy[1,2], D. J. Jones[1,2], C. Giannetti[5,6] and A. Damascelli[1,2]*

The possibility of driving phase transitions in low-density condensates through the loss of phase coherence alone has far-reaching implications for the study of quantum phases of matter. This has inspired the development of tools to control and explore the collective properties of condensate phases via phase fluctuations. Electrically gated oxide interfaces[1,2], ultracold Fermi atoms[3,4] and cuprate superconductors[5,6], which are characterized by an intrinsically small phase stiffness, are paradigmatic examples where these tools are having a dramatic impact. Here we use light pulses shorter than the internal thermalization time to drive and probe the phase fragility of the $Bi_2Sr_2CaCu_2O_{8+\delta}$ cuprate superconductor, completely melting the superconducting condensate without affecting the pairing strength. The resulting ultrafast dynamics of phase fluctuations and charge excitations are captured and disentangled by time-resolved photoemission spectroscopy. This work demonstrates the dominant role of phase coherence in the superconductor-to-normal state phase transition and offers a benchmark for non-equilibrium spectroscopic investigations of the cuprate phase diagram.

The value of the critical temperature (T_c) in a superconducting material is controlled by the interplay of two distinct phenomena: the formation of electron pairs and the onset of macroscopic phase coherence. While the pairing energy (E_p) is generally controlled by the bosonic modes that mediate the electronic interactions[7,8], the macroscopic phase Θ depends on the stability of the condensate against fluctuations and inhomogeneities. The energy scale relevant for phase fluctuations can be expressed via the Ginzburg–Landau theory as $\hbar\Omega_\Theta = [\hbar^2 n_S(0)a]/2m^*$, where m^* is the effective mass of the pairs, a is a characteristic length and $n_S(0)$ is the zero-temperature superfluid density. In conventional superconductors $E_p \ll \hbar\Omega_\Theta$ and therefore T_c is determined solely by thermal charge excitations across the superconducting gap, which act to reduce the number of states available for the formation of the superconducting condensate.

In cuprate superconductors, the scenario is much more complex since the small superfluid density pushes $\hbar\Omega_\Theta$ down to a value that is very close to the pairing energy[5]: the low density of the quasi-two-dimensional condensate within the Cu–O planes depresses $\hbar\Omega_\Theta$ as low as ~15 meV in bismuth-based copper oxides[5,9]. Several equilibrium measurements on underdoped cuprate superconductors have

reported a non-zero pairing gap up to $T \approx 1.5 \times T_c$ (refs [10,11]) even in the absence of macroscopic phase coherence. On heating for example, high-resolution angle-resolved photoemission (ARPES) experiments have shown pair-breaking scattering phenomena to emerge sharply at T_c while the pairing gap is still open, suggesting a direct connection between pair-breaking and the onset of the phase fluctuations[12,13]. In the same temperature range, non-equilibrium optical and terahertz experiments have given evidence for picosecond dynamics dominated by phase fluctuations above T_c (refs [6,14,15]).

The present work is motivated by the idea that a light pulse shorter than the internal thermalization time may be used to manipulate the density of phase fluctuations in a high-T_c superconductor independent of the number of across-gap charge excitations. This would open the possibility of investigating a transient regime inaccessible at equilibrium, where both phase fluctuations and charge excitations are controlled by the same temperature and thus inherently locked. Here we demonstrate this concept in the underdoped $Bi_2Sr_2CaCu_2O_{8+\delta}$ (Bi2212) superconductor ($T_c \sim 82$ K)[16,17]. Time- and angle-resolved photoemission spectroscopy (TR-ARPES) is used to evaluate the electronic spectral function that encodes information regarding the pair-breaking dynamics. We demonstrate that the pair-breaking scattering rate Γ_p, which is experimentally[12,13] and microscopically[18–20] associated with the scattering of phase fluctuations, is indeed decoupled from the dynamics of the pairing gap and across-gap charge excitations. At and above the critical fluence $F_C \approx 15\,\mu J\,cm^{-2}$ (refs [21–23]), the increase of Γ_p is such that superconductivity is suppressed. Quantitatively, we observe that the non-thermal melting of the condensate[21–26] is achieved when $\Gamma_p \approx \hbar\Omega_\Theta$.

TR-ARPES provides direct snapshots of the one-electron removal spectral function $A(\mathbf{k},\omega)$ (ref. [27]) and its temporal evolution[28,29] due to the perturbation by an ultrashort pump pulse. The spectral function $A(\mathbf{k},\omega)$ depends on both the electron self-energy $\Sigma(\omega) = \Sigma'(\omega) + i\Sigma''(\omega)$ and the bare energy dispersion ϵ_k:

$$A(\mathbf{k},\omega) = -\frac{1}{\pi}\frac{\Sigma''(\omega)}{[\omega - \epsilon_k - \Sigma'(\omega)]^2 + [\Sigma''(\omega)]^2} \qquad (1)$$

For a superconductor, $\Sigma(\omega)$ at the Fermi momentum $k = k_F$ can be approximated well by
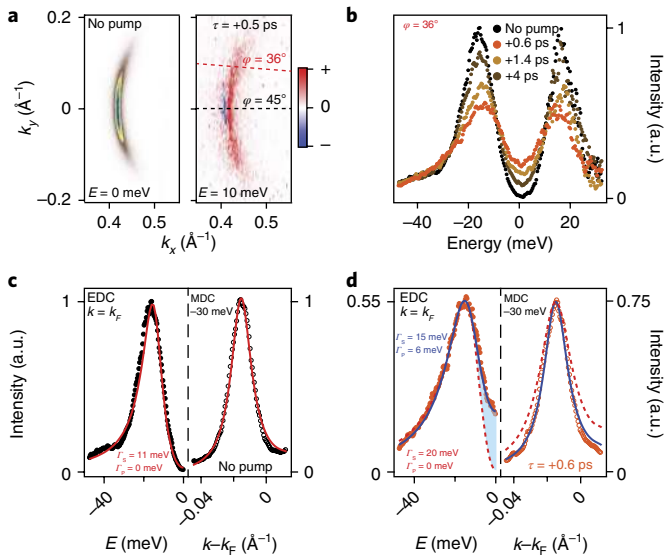
Fig. 1 | Ultrafast gap filling via enhancement of phase fluctuations. a, Equilibrium Fermi surface mapping (left panel) and differential (Pump$_{on}$−Pump$_{off}$) iso-energy contour mapping at 10 meV above the Fermi level E_F, 0.5 ps pump–probe delay (right panel). The integration energy range is 10 meV and k_x is aligned along the Γ–Y direction. The dashed black and red lines in the right panel define the nodal and off-nodal cuts investigated in the present work (details in Supplementary Information). **b**, Off-nodal EDC at $k = k_F$ ($\varphi = 36°$) normalized to momentum-integrated nodal EDC ($\varphi = 45°$) at different pump–probe delays, $F < F_C$ fluence ($F_C \approx 15\,\mu J\,cm^{-2}$). EDCs have been deconvoluted from the energy resolution broadening before the division[35] (details in Supplementary Information). **c**, Equilibrium off-nodal ($\varphi = 36°$) normalized EDC at k_F (left panel) and MDC at $E = -30$ meV (right panel). The solid lines represent the best fit to the data. The EDC and MDC have been simultaneously fitted using a global procedure. Equations (1) and (2) are fitted to the EDC, while a phenomenological Lorentzian is fitted to the MDC deconvoluted from energy and angular resolutions, as well as contributions not accounted for due to the assumption of frequency-independent scattering terms in equation (2). The equilibrium curve is well reproduced by $\Gamma_s = 11.0 \pm 0.5$ meV and $\Gamma_p \approx 0$ meV (red line). **d**, Non-equilibrium off-nodal ($\varphi = 36°$) EDC and MDC as measured at a delay of 0.6 ps. The solid blue lines represent the outcome of the global fitting procedure, which gives $\Gamma_s = 15.0 \pm 0.5$ meV and $\Gamma_p = 6 \pm 1$ meV. The red dashed lines represent the curves obtained when Γ_p is constrained to zero and Γ_s is left as the only free parameter for the EDC fit non-benchmarked against the MDC. The transparent blue area highlights the filling of the superconducting gap induced by a sizable Γ_p.

$$\Sigma(\omega) = -i\Gamma_s + \frac{\Delta^2}{(\omega + i\Gamma_p)} \qquad (2)$$

where Δ is the superconducting gap amplitude, Γ_s the single-particle scattering rate and Γ_p the pair-breaking scattering rate, as proposed in ref. [18]. When the condensate is fully coherent (that is, for $T \ll T_c$ at equilibrium), the pair-breaking scattering rate Γ_p is expected to vanish. This term may be interpreted as relating to the finite lifetime of a Cooper pair as a result of scattering from phase fluctuations[18–20].

To begin, we focus on the temporal evolution of the near-nodal superconducting gap. In Fig. 1a we display a section of the Bi2212 Fermi surface (left panel) and the differential iso-energy contour map (right panel). The latter is obtained by subtracting the equilibrium iso-energy contour at 10 meV (above the Fermi energy, E_F) from its counterpart obtained at 0.5 ps pump–probe delay. This differential shows a clear in-gap signal that has been previously related

to the quasiparticle recombination dynamics and the pairing gap closure[21–23,30,31]. To then study the pairing gap dynamics, it is common to fit symmetrized energy distribution curves (SEDCs) at $k = k_F$ (refs [18,21,32]). Although the emergence of a single peak in the SEDCs at large enough excitation fluences in TR-ARPES has been interpreted as a signature of the pump-induced gap closure[21,23], the comprehensive analysis of our data presented in the following provides clear evidence that a single peak in the SEDCs is instead related to the filling of an almost unperturbed pairing gap[12,13,33]. This provides consistency between transient and equilibrium studies, offering a coherent picture of the electronic structure and its related dynamics.

Before proceeding to the detailed modelling and quantitative analysis of the data, we address the microscopic origins of the evolution of the transient spectral function. We emphasize those photoinduced modifications to the spectral function that are immediately apparent, even at the level of visual inspection. In Fig. 1b we present the temporal evolution of the low-fluence EDC at $k = k_F$ along the off-nodal direction ($\varphi = 36°$), normalized to the momentum-integrated nodal EDC (both deconvoluted from the energy resolution broadening before the division, see Supplementary Section II). Without invoking controversial symmetrization, this procedure allows us to explore the spectral function and its dynamics both below and above the superconducting gap. The resulting curves in Fig. 1b provide direct evidence for the particle–hole symmetry of the quasiparticle states across the superconducting gap in the near-nodal region (that is, where pseudogap contributions are negligible[34–36]). Most importantly, the data in Fig. 1b reveal that the gap size (peak-to-peak distance) remains almost constant over the entire domain of time-delays measured. In contrast to this, we observe a transient decrease and broadening of the quasiparticle peak on either side of the gap, leading to a filling of spectral weight inside the superconducting gap (analogous conclusions are reached by a complementary analysis of the tomographic density of states[13], as shown in Supplementary Section III).

For a more quantitative analysis, we can model the TR-ARPES data in terms of equations (1) and (2). In principle, the in-gap broadening of the spectral function could be caused by both Γ terms in equation (2), and so we have developed a global analysis of the EDCs and momentum-distribution curves (MDCs), which stabilizes the fitting procedure and achieves consistency across our results for all delays and excitation fluences (Supplementary Section IV). In Fig. 1c we show the result of this global fitting at negative delays. The best simultaneous fit to EDC and MDC returns $\Gamma_s = 11.0 \pm 0.5$ meV and $\Gamma_p \approx 0$ meV, which are consistent with the equilibrium values extracted from conventional ARPES[12]. At positive delays (see the spectra at $\tau = 0.6$ ps in Fig. 1d as a typical example), the filling of spectral weight inside the gap modifies the spectral lineshape such that even a qualitative fit requires the introduction of a non-zero Γ_p. Quantitatively, the sensitivity of the MDC lineshape to small variations of Γ_s allows us to retrieve the values of the scattering rates at each time delay. This can be extended to consider even those excitations sufficiently large to induce complete filling of the gap in spectral weight near E_F.

We now move to the analysis of the temporal dynamics of Γ_p. For the sake of simplicity—and having experimentally verified particle–hole symmetry across the gap in the momentum range of interest—we analyse the SEDCs, which are not influenced by the effects of thermal broadening[32] or the low signal-to-noise ratio for states above E_F, as in Fig. 1. In Fig. 2a we present the temporal evolution of the SEDCs along the off-nodal cut ($\varphi = 36°$) at two different excitation fluences, $F < F_C$ and $F > F_C$, where F_C is the critical fluence for which the SEDCs exhibit a single envelope centred at the E_F (refs [22,23,37]). For both fluences employed, the global fit approach described above provides an accurate and reliable determination of the temporal evolution of Γ_s as well as Δ and Γ_p (Fig. 2b,c). While the gap amplitude (Δ) does not show a significant reduction for any
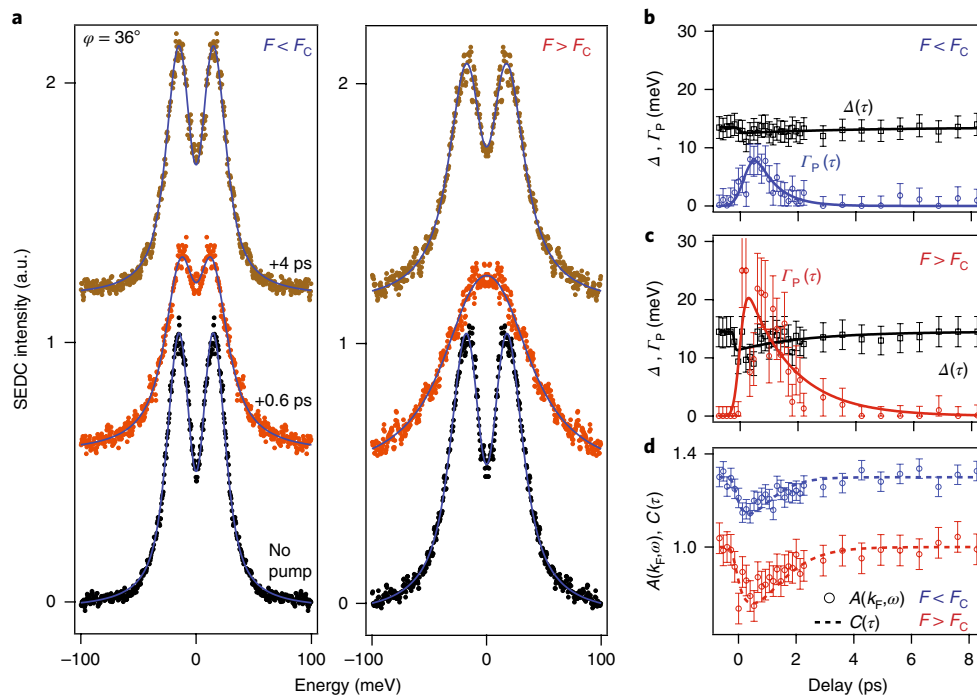
Fig. 2 | Temporal evolution of the spectral function via SEDC–MDC global analysis. a, SEDCs at $k = k_F$, off-nodal cut $\varphi = 36°$. SEDCs have been fitted using the global procedure described in the main text and Supplementary Information (blue lines). **b,c**, Ultrafast dynamics of Δ and the pair-breaking term, Γ_p, resulting from the global analysis of the SEDCs (shown in **a**) and MDCs. Pump excitation fluences are defined as $F < F_C$ (**b**) and $F > F_C$ (**c**). The solid lines are a phenomenological fit to a bi-exponential function convolved with a Gaussian accounting for the temporal resolution. **d**, Temporal evolution of the amplitude of the spectral function at $k = k_F$ (normalized at $\tau < 0$ ps, circles) and of the phenomenological function $C(\tau)$ as defined in the main text (dashed lines). Error bars in **b**–**d** define the confidence interval of the global procedure.

excitation fluence, the leading term that drives the dynamics, and eventually the complete filling of spectral weight inside the gap, is the enhancement of Γ_p as triggered by the pump excitation.

As an interesting consequence, we note that the dynamics of the quasiparticle spectral weight (circles in Fig. 2d) can be mapped onto the phenomenological function $C(\tau) = \frac{1}{2}[1 + e^{-\frac{\Gamma_p(\tau)}{\Gamma_S(\tau)}}]$ (dashed lines in Fig. 2d), which resembles the momentum-averaged two-particle scattering coherence factor[38,39]. This empirical relationship between the single-particle ARPES spectral weight and a two-particle correlator suggests an intriguing scenario in which the quasiparticle peak amplitude is intertwined with the condensate density. Such a relationship, already suggested by previous ARPES studies[37,40,41], calls for future experimental and theoretical investigations.

The viability of measuring the evolution of Γ_p in the time domain provides essential information regarding the intrinsic dynamics of condensate formation in the cuprates. Figure 3a,b shows that the Γ_p relaxation dynamics for $F < F_C$ are completely decoupled from those of the gap amplitude and of the above-gap charge excitations. In particular, in Fig. 3b we compare the temporal evolution of Γ_p (blue, obtained by fitting the data in Fig. 2b) with the dynamics of the superconducting gap (black, from Fig. 2b) and of the charge excitations (green, as obtained by integrating the off-nodal pump-induced charge population in the above-gap 15–70 meV energy window shown in the inset of Fig. 2b). While the temporal evolution of the above-gap excitations and that of the gap amplitude are locked to each other with a 4.0 ± 0.5 ps recovery time, Γ_p relaxes much faster with a relaxation rate $\tau_\Theta \approx 1$ ps. This value is of the same order of magnitude as the phase-correlation time extracted from high-frequency conductivity and related to the motion of topological defects[6].

Microscopically, the transient increase of phase fluctuations can be rationalized as a cascade process triggered by the optical pump, which initially breaks the electronic pairs and promotes hot

quasiparticles to energies well above E_F. During their decay, the non-thermal quasiparticle population can either couple directly to phase excitations or scatter off high-energy bosonic excitations on a timescale of tens (spin fluctuations) to hundreds (optical phonons) of femtoseconds[42–44]. The subsequent absorption of these bosons can break additional Cooper pairs. Furthermore, any pair recombination process must emit a gap-energy boson to satisfy energy conservation, as described by the Rothwarf–Taylor equations[26]. As a result, after a few hundred femtoseconds, the initial excitation is converted into a non-thermal bosonic population. We speculate that such highly energetic bosons, coupled to the fermionic bath, can interact even indirectly with the macroscopic condensate. These bosons can be considered as a possible source of the excess phase fluctuations that give a finite lifetime to the Cooper pairs. This picture is corroborated by the observation of a maximum change in Γ_p (Fig. 3a) approximately 500 fs after the pump excitation. Such a value is compatible with the build-up time observed via time-resolved optical spectroscopy and has been justified as the time necessary for the growth of the non-thermal gap-energy bosonic population[26].

Together, these observations imply that the pair-breaking processes related to the loss of coherence of the condensate can be decoupled from the charge excitations on the picosecond timescale. In this transient state, the condensate becomes more fragile, despite an almost unaffected pairing strength. This result has important consequences for establishing the nature of the instability of the macroscopic condensate at higher excitation fluences. Both time-resolved optical[24–26,45,46] and photoemission[21–23,30,33,37,47] experiments have measured the collapse of superconductivity and the complete quench of the coherence factor for pump fluence ranging from 14 to 70 μJ cm⁻². Our data demonstrate that at $F \geq 15$ μJ cm⁻², the non-equilibrium pair-breaking rate becomes of the order of the energy scale relevant to phase fluctuations—that is, $\Gamma_p \approx \hbar\Omega_\Theta \approx 15$ meV (Fig. 2b),
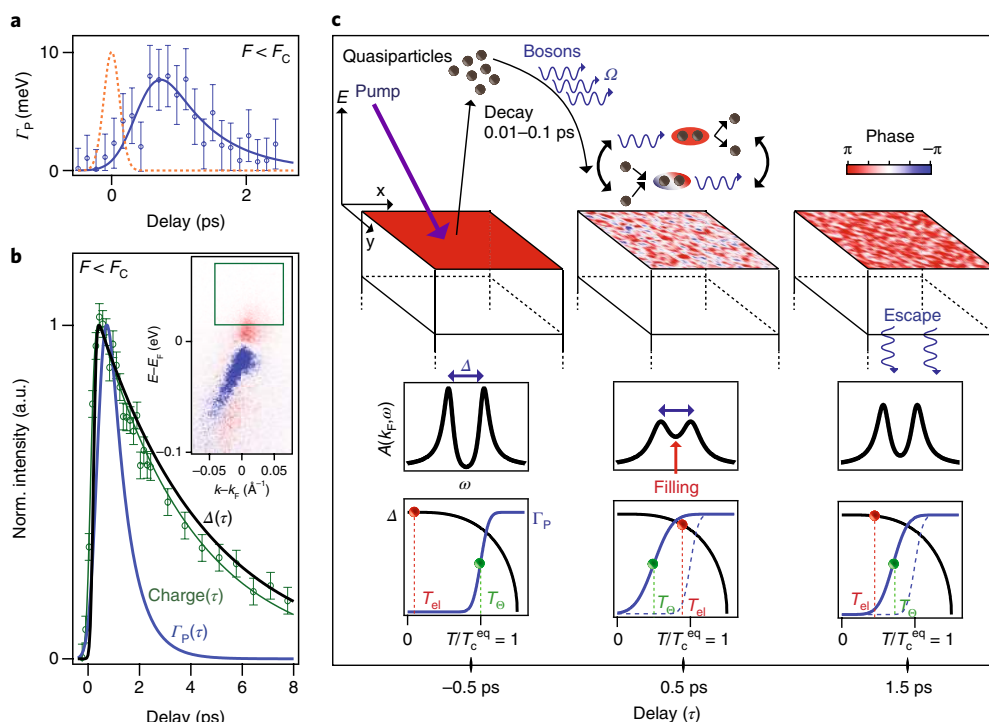
Fig. 3 | Role of phase fluctuations in the transient collapse of the condensate. a, Γ_p dynamics for $F < F_C$ (blue circles, error bars defined in Fig. 2; the blue line is the phenomenological fit described in Fig. 2), compared with the pump–probe cross-correlation (orange dashed line). **b**, Comparison, again for $F < F_C$, of the normalized differential dynamics calculated as $[a(\tau) - a(\tau < 0)]/\max[a(\tau)]$, for Γ_p (blue line, from data in Fig. 2b), Δ (black line, from data in Fig. 2b) and charge dynamics (green circles obtained from the integrated off-nodal pump-induced population in the above-gap 15–70 meV energy window—highlighted area in the inset—and corresponding exponential fit; error bars represent the systematic errors associated with the experiment). **c**, Pictorial sketch of the transient collapse of the condensate: a non-equilibrium bosonic population induces phase fluctuations leading to a gap filling and a modification of the temperature where the phase coherence is set independently to the charge dynamics. The top panels show a schematic diagram of the energetics of the process and the related real-space condensate phase coherence; the middle panels display the spectral function at $k = k_F$ when phase fluctuations are induced; the bottom panels show the temporal evolution of the pairing strength Δ (gap amplitude, black line) and of the pair-breaking scattering rate Γ_p (blue line). While the pairing is controlled by the electronic temperature T_{el} (red spheres and dashed lines), and has an onset higher than T_c itself, superconductivity and the macroscopic T_c are determined by the onset of phase coherence at $T_\Theta \approx \hbar\Omega_\Theta/k_B$ (green spheres and dashed lines).

which corresponds to a Cooper pair lifetime of ≈40 fs. Figure 3c provides a pictorial illustration of the dynamics of the superconductor-to-normal state phase transition: the transient excess of phase fluctuations driven by highly energetic bosons fills the superconducting gap and does not affect the pairing strength. We emphasize that while these results are consistent with the notion of preformed Cooper pairs and that sufficient enhancement of Γ_p could culminate in the evolution of Fermi arcs[18,48], the limited region of momentum space explored in this current work precludes any discussion of the pseudogap state.

These results challenge the current understanding of the superconducting phase transition in cuprates. The TR-ARPES data presented here constitute direct evidence that the phase coherence controls the condensate formation in underdoped high-T_c superconductors, while the temperature-driven occupation of states plays a secondary role[5]. Indeed, our results demonstrate that the recovery of phase coherence is the primary and fastest mechanism by which we restore superconductivity (see Fig. 3b). In addition, the ability to melt the condensate without altering the gap size or increasing the electronic temperature substantively (Fig. 3c) suggests spectroscopic explorations of the hierarchy of pairing and phase coherence throughout the cuprate phase diagram, and in the vicinity of the putative quantum critical points[49]. Further investigation and the development of selective excitation schemes will be essential to test possible interpretations of the dynamical response of the phase coherence in high-T_c superconductors. In particular, a detailed study of the

frequency dependence of Γ_p may elucidate the microscopic mechanism responsible for the enhancement of phase fragility reported here. Furthermore, by extending these techniques to other members of the cuprate family, the relative role of dimensionality and interlayer coupling in the transient quenching of the superconducting condensate may be established[5,50]. The mechanism by which fermions interact with phase modes and how gap-energy bosons interact with the pair condensate toward the ultimate result of a plasma of incoherent excitations still remains as an open and intriguing issue.

Methods

Methods, including statements of data availability and any associated accession codes and references, are available at https://doi.org/10.1038/s41563-018-0045-1.

References

1. Caviglia, A. D. et al. Electric field control of the LaAlO$_3$/SrTiO$_3$ interface ground state. *Nature* **456**, 624–627 (2008).
2. Hwang, H. Y. et al. Emergent phenomena at oxide interfaces. *Nat. Mater.* **11**, 103–113 (2012).
3. Regal, C. & Jin, D. Experimental realization of the BCS-BEC crossover with a Fermi gas of atoms. *Adv. At. Mol. Opt. Phys.* **54**, 1–79 (2007).
4. Gaebler, J. P. et al. Observation of pseudogap behaviour in a strongly interacting Fermi gas. *Nat. Phys.* **6**, 569–573 (2010).

5. Emery, V. J. & Kivelson, S. A. Importance of phase fluctuations in superconductors with small superfluid density. *Nature* **374**, 434–437 (1995).

6. Corson, J., Mallozzi, R., Orenstein, J., Eckstein, J. N. & Bozovic, I. Vanishing of phase coherence in underdoped $Bi_2Sr_2CaCu_2O_{8+δ}$. *Nature* **398**, 221–223 (1999).

7. Johnston, S. et al. Material and doping dependence of the nodal and antinodal dispersion renormalizations in single- and multilayer cuprates. *Adv. Condens. Matter Phys.* **2010**, 968304 (2010).

8. Kordyuk, V. et al. An ARPES view on the high-T_c problem: phonons vs. spin-fluctuations. *Eur. Phys. J. Spec. Top.* **188**, 153–162 (2010).

9. Benfatto, L., Caprara, S., Castellani, C., Paramekanti, A. & Randeria, M. Phase fluctuations, dissipation, and superfluid stiffness in d-wave superconductors. *Phys. Rev. B* **63**, 174513 (2001).

10. Wang, Y. et al. Onset of the vortexlike Nernst signal above T_c in $La_{2-x}Sr_xCuO_4$ and $Bi_2Sr_{2-y}La_yCuO_6$. *Phys. Rev. B* **64**, 224519 (2001).

11. Li, L. et al. Diamagnetism and Cooper pairing above T_c in cuprates. *Phys. Rev. B* **81**, 054510 (2010).

12. Kondo, T. et al. Point nodes persisting far beyond T_c in Bi2212. *Nat. Commun.* **6**, 7699 (2015).

13. Reber, T. J. et al. The origin and non-quasiparticle nature of Fermi arcs in $Bi_2Sr_2CaCu_2O_{8+δ}$. *Nat. Phys.* **8**, 606–610 (2012).

14. Madan, I. et al. Separating pairing from quantum phase coherence dynamics above the superconducting transition by femtosecond spectroscopy. *Sci. Rep.* **4**, 5656 (2014).

15. Perfetti, L. et al. Ultrafast dynamics of fluctuations in high-temperature superconductors far from equilibrium. *Phys. Rev. Lett.* **114**, 067003 (2015).

16. Gomes, K. K. et al. Mapping of the formation of the pairing gap in $Bi_2Sr_2CaCu_2O_{8+δ}$. *J. Phys. Chem. Solids* **69**, 3034–3038 (2008).

17. Ding, H. et al. Angle-resolved photoemission spectroscopy study of the superconducting gap anisotropy in $Bi_2Sr_2CaCu_2O_{8+x}$. *Phys. Rev. B* **54**, R9678–R9681 (1996).

18. Norman, M. R., Randeria, M., Ding, H. & Campuzano, J. C. Phenomenology of the low-energy spectral function in high-T_c superconductors. *Phys. Rev. B* **57**, R11093–R11096 (1998).

19. Franz, M. & Millis, A. J. Phase fluctuations and spectral properties of underdoped cuprates. *Phys. Rev. B* **58**, 14572–14580 (1998).

20. Kwon, H.-J. & Dorsey, A. T. Effect of phase fluctuations on the single-particle properties of underdoped cuprates. *Phys. Rev. B* **59**, 6438–6448 (1999).

21. Smallwood, C. L. et al. Tracking cooper pairs in a cuprate superconductor by ultrafast angle-resolved photoemission. *Science* **336**, 1137–1139 (2012).

22. Zhang, W. et al. Signatures of superconductivity and pseudogap formation in nonequilibrium nodal quasiparticles revealed by ultrafast angle-resolved photoemission. *Phys. Rev. B* **88**, 245132 (2013).

23. Smallwood, C. L. et al. Time- and momentum-resolved gap dynamics in $Bi_2Sr_2CaCu_2O_{8+δ}$. *Phys. Rev. B* **89**, 115126 (2014).

24. Kusar, P. et al. Controlled vaporization of the superconducting condensate in cuprate superconductors by femtosecond photoexcitation. *Phys. Rev. Lett.* **101**, 227001 (2008).

25. Giannetti, C. et al. Discontinuity of the ultrafast electronic response of underdoped superconducting $Bi_2Sr_2CaCu_2O_{8+δ}$ strongly excited by ultrashort light pulses. *Phys. Rev. B* **79**, 224502 (2009).

26. Giannetti, C. et al. Ultrafast optical spectroscopy of strongly correlated materials and high-temperature superconductors: a non-equilibrium approach. *Adv. Phys.* **65**, 58–238 (2016).

27. Damascelli, A., Hussain, Z. & Shen, Z.-X. Angle-resolved photoemission studies of the cuprate superconductors. *Rev. Mod. Phys.* **75**, 473–541 (2003).

28. Sentef, M. et al. Examining electron-boson coupling using time-resolved spectroscopy. *Phys. Rev. X* **3**, 041033 (2013).

29. Kemper, A. F., Sentef, M. A., Moritz, B., Devereaux, T. P. & Freericks, J. K. Review of the theoretical description of time-resolved angle-resolved photoemission spectroscopy in electron–phonon mediated superconductors. *Ann. Phys.* **529**, 1600235 (2017).

30. Ishida, Y. et al. Quasi-particles ultra-fastly releasing kink bosons to form Fermi arcs in a cuprate superconductor. *Sci. Rep.* **6**, 18747 (2016).

31. Zhang, W. et al. Stimulated emission of Cooper pairs in a high-temperature cuprate superconductor. *Sci. Rep.* **6**, 29100 (2016).

32. Norman, M. R. et al. Destruction of the Fermi surface in underdoped high-T_c superconductors. *Nature* **392**, 157–160 (1998).

33. Parham, S. et al. Ultrafast gap dynamics and electronic interactions in a photoexcited cuprate superconductor. *Phys. Rev. X* **7**, 041013 (2017).

34. Matsui, H. et al. BCS-like Bogoliubov quasiparticles in high-T_c superconductors observed by angle-resolved photoemission spectroscopy. *Phys. Rev. Lett.* **90**, 217002 (2003).

35. Yang, H.-B. et al. Emergence of preformed Cooper pairs from the doped Mott insulating state in $Bi_2Sr_2CaCu_2O_{8+δ}$. *Nature* **456**, 77–80 (2008).

36. Hashimoto, M., Vishik, I. M., He, R.-H., Devereaux, T. P. & Shen, Z.-X. Energy gaps in high-transition-temperature cuprate superconductors. *Nat. Phys.* **10**, 483–495 (2014).

37. Graf, J. et al. Nodal quasiparticle meltdown in ultrahigh-resolution pump-probe angle-resolved photoemission. *Nat. Phys.* **7**, 805–809 (2011).

38. Hanaguri, T. et al. Coherence factors in a high-T_c cuprate probed by quasi-particle scattering off vortices. *Science* **323**, 923–926 (2009).

39. Hinton, J. P. et al. The rate of quasiparticle recombination probes the onset of coherence in cuprate superconductors. *Sci. Rep.* **6**, 23610 (2016).

40. Feng, D. L. et al. Signature of superfluid density in the single-particle excitation spectrum of $Bi_2Sr_2CaCu_2O_{8+δ}$. *Science* **289**, 277–281 (2000).

41. Ding, H. et al. Coherent quasiparticle weight and its connection to high-T_c superconductivity from angle-resolved photoemission. *Phys. Rev. Lett.* **87**, 227001 (2001).

42. Dal Conte, S. et al. Snapshots of the retarded interaction of charge carriers with ultrafast fluctuations in cuprates. *Nat. Phys.* **11**, 421–426 (2015).

43. Perfetti, L. et al. Ultrafast electron relaxation in superconducting $Bi_2Sr_2CaCu_2O_{8+δ}$ by time-resolved photoelectron spectroscopy. *Phys. Rev. Lett.* **99**, 197001 (2007).

44. Rameau, J. D. et al. Energy dissipation from a correlated system driven out of equilibrium. *Nat. Commun.* **7**, 13761 (2016).

45. Averitt, R. D. et al. Nonequilibrium superconductivity and quasiparticle dynamics in $YBa_2Cu_3O_{7-δ}$. *Phys. Rev. B* **63**, 140502 (2001).

46. Kaindl, R. A., Carnahan, M. A., Chemla, D. S., Oh, S. & Eckstein, J. N. Dynamics of Cooper pair formation in $Bi_2Sr_2CaCu_2O_{8+δ}$. *Phys. Rev. B* **72**, 060510 (2005).

47. Zhang, Z. et al. Photoinduced filling of near-nodal gap in $Bi_2Sr_2CaCu_2O_{8+δ}$. *Phys. Rev. B* **96**, 064510 (2017).

48. Chubukov, A. V., Norman, M. R., Millis, A. J. & Abrahams, E. Gapless pairing and the Fermi arc in the cuprates. *Phys. Rev. B* **76**, 180501 (2007).

49. Sachdev, S. *Quantum Phase Transitions* (Cambridge Univ. Press, Cambridge, UK, 2000).

50. Baldini, E. et al. Clocking the onset of bilayer coherence in a high-T_c cuprate. *Phys. Rev. B* **95**, 024501 (2017).

Acknowledgements

Author contributions

F.B., E.H.d.S.N., D.J.J., C.G. and A.D. conceived the investigation. F.B. performed TR-ARPES measurements with the assistance of E.H.d.S.N., E.R. and M.Z., and F.B., E.H.d.S.N., E.R., M.Z., S.P., R.P.D., M.M., M.S., B.Z., P.N., S.Z., A.K.M. and G.L. were responsible for operation and maintenance of the experimental system. F.B., E.H.d.S.N., E.R., C.G. and A.D. were responsible for data analysis and interpretation. R.D.Z., J.S. and G.D.G. provided Bi2212 samples. All of the authors discussed the underlying physics and contributed to the manuscript. F.B., E.H.d.S.N., R.P.D., C.G. and A.D. wrote the manuscript. A.D. was responsible for the overall direction, planning and management of the project.

Competing interests

The authors declare no competing interests.

Additional information

Methods

Experimental set-up. Our TR-ARPES system is based on a Ti:sapphire laser (VitesseDuo + RegA 9000 by Coherent) delivering 800 nm pulses (1.55 eV) with a 180 fs pulse duration, and 250 kHz repetition rate. The output beam is split: a portion is used as the pump beam while the remaining part generates its fourth harmonic, that is, 200 nm (6.2 eV). The 6.2 eV is generated through a cascade of nonlinear processes. The probe (6.2 eV) and the pump (1.55 eV) beams are both vertically (s) polarized and they are focused onto the sample (45° angle of incidence) using the same focusing optic, leading to approximately 120 μm and 250 μm spot sizes, respectively. The ARPES measurements are conducted in ultrahigh vacuum with a base pressure lower than 3×10^{-11} torr, at a base temperature of 6 K. The angle and energy of the photoelectrons are resolved using a SPECS Phoibos 150 electron analyser. The momentum, energy and temporal resolutions of the system are <0.003 Å^{-1}, 19 meV and 250 fs, respectively, referenced from polycrystalline gold. Incident pump fluences indicated as $F < F_C$ and $F > F_C$ correspond to 8 ± 2 μJ cm^{-2} and 30 ± 4 μJ cm^{-2}, respectively.

Samples. Single-crystal Bi$_2$Sr$_2$CaCu$_2$O$_{8+\delta}$ (Bi2212) samples have been grown using the floating-zone method and hole-doped by oxygen annealing ($T_c \simeq 82$ K). Bi2212 samples have been characterized by scanning tunneling microscopy measurements[16], and the gap amplitude extracted from the global fitting procedure agrees well with that reported elsewhere[17].

Data availability. The data that support the plots within this paper and other findings of this study are available from the corresponding author upon reasonable request.